

光学学报

基于 Rydberg 原子的 100 kHz~40 GHz 超宽带射频传感器

杨凯, 安强, 姚佳伟, 毛瑞祺, 林沂*, 刘燚**, 付云起***

国防科技大学电子科学学院电子科学系, 湖南 长沙 410073

摘要 Rydberg 原子具有极大的极化率和跃迁偶极矩, 利用谐振区的 Autler-Townes 分裂效应和非谐振区的交流斯塔克 (AC Stark) 偏移效应, 可以实现超宽带电磁信号无损可溯源的精密测量与通信。在室温铯原子气室中, 通过改变耦合光波长, 选用 $|70S_{1/2}\rangle$, $|42D_{5/2}\rangle$ 和 $|30D_{5/2}\rangle$ 三个不同的 Rydberg 能级, 分别测量了远失谐区 (2 GHz) 和谐振区 (9.953 GHz 和 29.54 GHz) 电磁信号的空间电场强度, 并由此计算出环境散射和气室扰动所产生的衰减因子。同时, 实验展示了 Rydberg 原子在宽带频率范围内的通信应用潜力, 研究了远失谐区 (2 GHz)、近失谐区 (9.5 GHz) 和谐振区 (29.54 GHz) 电磁信号在不同调制频率下幅度调制和频率调制的信噪比 (SNR), 并在此基础上, 测量了调制频率为 10 kHz 的幅度调制信号在 100 kHz~40 GHz 超宽带频率范围内的解调信号 SNR。实验结果表明, Rydberg 原子可以突破传统电子学传感器的工作带宽限制, 在超宽带连续频谱范围内具有电场感知与通信能力。

关键词 传感器; Rydberg 原子; 超宽带; 电场测量; 通信

中图分类号 O469 文献标志码 A

DOI: 10.3788/AOS202242.1528002

Rydberg Atom-Based Ultra-Broadband Radio Frequency Sensor from 100 kHz to 40 GHz

Yang Kai, An Qiang, Yao Jiawei, Mao Ruiqi, Lin Yi*, Liu Yi**, Fu Yunqi***

Department of Electronic Science and Technology, College of Electronic Science and Technology, National University of Defense Technology, Changsha 410073, Hunan, China

Abstract Rydberg atoms have extremely large polarizability and transition dipole moments, allowing for non-destructive and traceable precise measurement or communications over ultra-broadband electromagnetic signals by the Autler-Townes splitting effect in the resonance region and the alternating current Stark (AC Stark) shift effect in the off-resonance region. In a cesium vapor cell at room temperature, by varying the coupling laser wavelength, three energy levels ($|70S_{1/2}\rangle$, $|42D_{5/2}\rangle$, and $|30D_{5/2}\rangle$) are selected to measure the spatial electric field strength of electromagnetic signals in the far-off-resonance region (2 GHz) and the resonance region (9.953 GHz and 29.54 GHz), respectively. On this basis, the attenuation factors caused by environment scattering and vapor cell perturbations are calculated. Meanwhile, the potential of Rydberg atoms for communication applications in the broadband frequency range is demonstrated by experiments on the variation of the signal-to-noise ratios (SNRs) of electromagnetic signals with different modulation frequencies under amplitude modulation and frequency modulation in the far-off-resonance region (2 GHz), near-off-resonance region (9.5 GHz), and the resonance region (29.54 GHz). Furthermore, for the amplitude modulation signal with a modulation frequency of 10 kHz, the demodulated signal SNR is investigated in the ultra-broadband frequency range of 100 kHz~40 GHz. The experimental results reveal that Rydberg atoms can break the operational bandwidth limit of conventional electronic sensors, and have the ability of electric field sensing and communications in the ultra-broadband continuous spectrum range.

Key words sensors; Rydberg atoms; ultra-broadband; electric field measurement; communication

收稿日期: 2022-01-07; 修回日期: 2022-02-08; 录用日期: 2022-02-23

基金项目: 国家自然科学基金(12104509, 61901495)

通信作者: *linyi@nudt.edu.cn; **yi_liu@nudt.edu.cn; ***yunqifu@nudt.edu.cn

1 引言

传统电子学传感器受限于Chu极限^[1],其物理尺寸与待测场的波长相当,且工作带宽窄,需根据待测场的频率更换不同天线。Rydberg原子具有极大的极化率(n^7)和微波跃迁偶极矩(n^2),对外部电磁场极为敏感^[2],以Rydberg原子为基础的新型量子传感器可以突破传统电子学传感器的工作带宽限制,实现超宽带电磁频段的全光无损探测。

近10年来,以Rydberg原子为基础的量子传感器研究方兴未艾。2012年,Sedlacek等^[3]利用微波耦合相邻Rydberg能级产生的Autler-Townes(AT)分裂效应在实验上实现了灵敏度为 $30\text{ }\mu\text{V}\cdot\text{cm}^{-1}\cdot\text{Hz}^{-1/2}$ 的微波电场强度测量。随后,他们利用马赫-曾德尔干涉仪和零差探测技术将测量灵敏度提高至 $5\text{ }\mu\text{V}\cdot\text{cm}^{-1}\cdot\text{Hz}^{-1/2}$ ^[4]。此方法通过测量两个分裂峰的频率宽度来得到所测的电场场强,测量结果可以追溯至普朗克常数,具有自校准的优势,但此方法的测量精度受限于电磁感应透明(EIT)光谱的线宽,无法探测更微弱的电场。利用冷原子技术^[5]、三光子电磁诱导吸收(EIA)^[6-8]、Rydberg原子外差^[9-12]、待测电场幅度调制^[13]、外加辅助电场缀饰Rydberg能级^[14-16]、再泵浦激光提高可作用原子数^[17]和谐振腔增强原子气室区域场强^[18]等方法可以压窄探测光谱线宽,提高电场测量灵敏度。除了具有电场强度测量能力之外,Rydberg量子传感器还可以探测电磁场的极化^[19]、频率^[20]、相位^[21-22]和来波方向^[23]等信息。利用Rydberg原子的多电磁场参数探测能力,人们将Rydberg量子传感器的应用拓展到诸如电场探针^[24-26]、立体声播放器^[27]、频谱分析仪^[28-29]和具备解调幅度(AM)^[30-32]、频率(FM)^[33-34]或者相位^[35]调制信号能力的通信接收机等领域中。

Rydberg原子能够响应频率为千赫兹至太赫兹水平的电磁信号^[36-38],但上述报道大都基于原子的谐振能级进行单个频点研究^[3-14]。通常有两种方法来拓展Rydberg原子传感器的响应带宽:第一种方法是改变耦合光波长使碱金属原子处于不同的Rydberg能级以响应不同的微波频率^[25, 27-28, 33],这种方法简单直接,理论上的工作频率跨度很大,但其工作频点都是离散的;第二种方法是通过辅助微波场缀饰Rydberg能级来展宽工作带宽^[16, 29],这种方法可以对一段连续的电磁频带作出响应,但实验要求相对严格,需要针对每个工作频点来调节辅助场的频率和功率甚至激光功率。

本文充分利用Rydberg原子在谐振区与非谐振区对外部电磁场的不同响应,选取 $|70S_{1/2}\rangle$ 、 $|42D_{5/2}\rangle$ 和 $|30D_{5/2}\rangle$ 三个不同的Rydberg能级,利用非谐振区的交流斯塔克(AC Stark)频移效应测量了2 GHz处的微波场强,利用谐振区的AT效应测量了9.953 GHz和29.54 GHz处的微波场强,并由此计算出空间散射和气室内驻波扰动所产生的衰减因子。同时,研究了远失谐区(2 GHz)、近失谐区(9.5 GHz)和谐振区(29.54 GHz)不同调制频率下AM信号和FM信号的

解调信噪比(SNR)。在此基础上,进一步地用10 kHz的AM调制信号验证了Rydberg量子传感器在100 kHz~40 GHz的超宽带频率范围内的连续响应能力。

2 实验装置

实验装置和相应的双光子跃迁阶梯EIT能级如图1(a)和图1(b)所示,其中DM为二向色镜,PBS为偏振分束棱镜,HR为介质反射镜,RF为射频。在室温下,一束波长为852 nm的弱探测光和一束波长为510 nm左右的强耦合光相向作用于一个直径为1 cm、长度为2 cm的圆柱形铯原子气室,探测光将原子从 $|6S_{1/2}, F=4\rangle$ 共振激发到 $|6P_{3/2}, F'=5\rangle$,耦合光将原子从 $|6P_{3/2}, F'=5\rangle$ 激发到不同的Rydberg态,其中F和F'为超精细能级。在实验中,选用 $|70S_{1/2}\rangle$ 态、 $|42D_{5/2}\rangle$ 态和 $|30D_{5/2}\rangle$ 态分别对2 GHz以下、2~20 GHz和20~40 GHz的电磁场进行探测。通过调节探测光(耦合光)的Rabi频率以获得高对比度的EIT光谱,这三种Rydberg态对应的探测光(耦合光)Rabi频率分别为 $\Omega_{p1}=2\pi\times 9.77\text{ MHz}$ ($\Omega_{c1}=2\pi\times 2.77\text{ MHz}$)、 $\Omega_{p2}=2\pi\times 8.91\text{ MHz}$ ($\Omega_{c2}=2\pi\times 17.75\text{ MHz}$)和 $\Omega_{p3}=2\pi\times 8.49\text{ MHz}$ ($\Omega_{c3}=2\pi\times 17.9\text{ MHz}$)。此外,频率覆盖100 kHz~40 GHz的空间电磁场可通过不同的装置产生:对于200 MHz以下的电磁场,用两个截面积为 $6\text{ cm}\times 15\text{ cm}$ 、间距为1.3 cm的平行板电极提供,气室放置于两个平行板电极的中间;对于200 MHz以上的电磁场,用商用八木天线或喇叭天线提供,并且外加电磁场的极化方向与两束激光的偏振方向平行。同时,探测光的频率用饱和吸收谱稳频法锁定为铯原子的 $|6S_{1/2}, F=4\rangle\rightarrow|6P_{3/2}, F'=5\rangle$ 跃迁频率^[39-40],扫描耦合光频率时可以得到EIT-AT或者AC Stark频移光谱。当耦合光的频率用另外一个铯原子气室锁定为相应的 $|6P_{3/2}, F'=5\rangle\rightarrow|\text{Rydberg}\rangle$ 跃迁频率时,Rydberg原子对外加调制电磁场的响应就可以通过探测光的光强变化直接反应在光电探测器上。

3 实验结果与讨论

3.1 电场强度测量

在外部电磁场作用下,通过测量Rydberg原子光谱的变化可以得到外部电场场强值。在谐振区中,电磁波通过耦合相邻Rydberg能级使得光谱产生EIT-AT分裂,当固定探测光频率,扫描耦合光频率时,电场强度 $|E|$ 与AT分裂间隔 ΔD_{AT} 的关系^[3]可以表示为

$$|E|=\frac{\hbar}{\mu}\Omega_{\text{MW}}=2\pi\frac{\hbar}{\mu}\Delta D_{\text{AT}}, \quad (1)$$

式中: \hbar 为约化普朗克常数; Ω_{MW} 为微波场的Rabi频率,AT分裂峰间距 ΔD_{AT} 与微波场Rabi频率 Ω_{MW} 的关系为 $\Omega_{\text{MW}}=2\pi\times\Delta D_{\text{AT}}$; μ 为两个Rydberg态之间的跃迁偶极矩。对于本文中用到的两个Rydberg态($|42D_{5/2}\rangle$ 和 $|30D_{5/2}\rangle$)来说,用9.953 GHz的电磁波耦

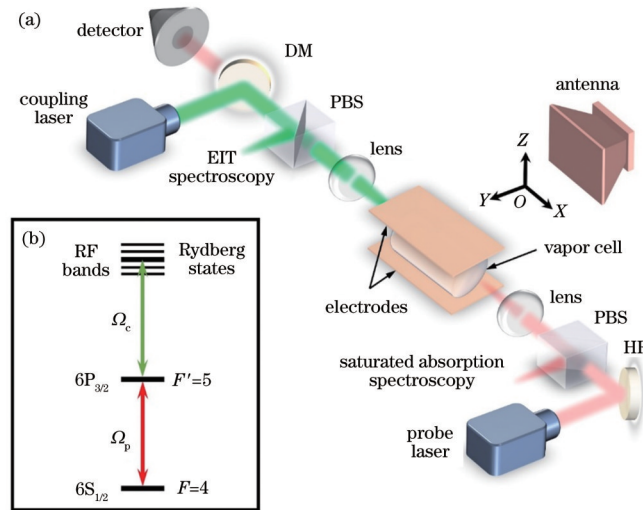


图1 实验装置与能级示意图。(a)实验装置图;(b)双光子跃迁阶梯Rydberg EIT能级示意图

Fig. 1 Experimental setup and energy-level diagram. (a) Diagram of experimental setup; (b) energy-level diagram of two-photon transition ladder Rydberg EIT

合 $|42D_{5/2}\rangle \rightarrow |43P_{3/2}\rangle$ 的共振跃迁,用29.54 GHz的电磁波耦合 $|30D_{5/2}\rangle \rightarrow |31P_{3/2}\rangle$ 的共振跃迁。

在远失谐区中,EIT光谱会在外加射频场的作用下发生AC Stark偏移,偏移量 ΔD_{Stark} 与外加电场场强E的二次方成正比^[26],可以表示为

$$\Delta D_{\text{Stark}} = -\frac{E^2}{4} \alpha_0 (2\pi \times f_{\text{MW}}), \quad (2)$$

式中: $\alpha_0(2\pi \times f_{\text{MW}})$ 是一个随频率变化的量,表示频率为 f_{MW} 处的动态标量极化率,一般来说,频率 f_{MW} 偏离谐振频率越远, $\alpha_0(2\pi \times f_{\text{MW}})$ 的值越小。

本实验中Rydberg原子在谐振区对9.953 GHz/29.54 GHz电磁波的响应和在远失谐区对2 GHz电磁波的响应如图2所示。图2(a)是9.953 GHz的电磁波在不同等效全向辐射功率(EIRP, $M_{\text{EIRP}} = P_t + G_t - L_r$, 其中 P_t 表示信号源输出功率, G_t 表示辐射天线增益, L_r 表示传输线插入损耗)下扫描耦合光频率产生的探测光幅度变化曲线。9.953 GHz的电磁波可以使铯原子从 $|42D_{5/2}\rangle$ 态共振跃迁到 $|43P_{3/2}\rangle$ 态,造成探测光谱的EIT-AT分裂,当信号强度变大时,AT峰的间隔随之增加,并且幅度缓慢下降。图2(b)是AT峰间隔 ΔD_{AT} 在不同EIRP的平方根 $\sqrt{M_{\text{EIRP}}}$ ($|E| \propto \sqrt{M_{\text{EIRP}}}$)下的测试数据和线性拟合曲线,可以看出, ΔD_{AT} 与 $\sqrt{M_{\text{EIRP}}}$ 之间存在良好的线性对应关系,与式(1)相吻合。图2(c)和图2(d)分别是铯原子在不同EIRP的29.54 GHz电磁波作用下 $|30D_{5/2}\rangle$ 和 $|31P_{3/2}\rangle$ 两个Rydberg态共振跃迁所形成的EIT-AT光谱和相应的 $\Delta D_{\text{AT}}-\sqrt{M_{\text{EIRP}}}$ 对应关系。与9.953 GHz电磁波作用情况不同的是,相同功率下29.54 GHz电磁波引起的AT峰间隔更小,光谱展宽更大,并且在谐振位置处出现了第三个探测光传输峰。相同功率下29.54 GHz电磁波引起的AT峰间隔更小的原因是 $|30D_{5/2}\rangle \rightarrow |31P_{3/2}\rangle$ 的跃迁偶极矩比 $|42D_{5/2}\rangle \rightarrow |43P_{3/2}\rangle$ 的跃迁偶极矩小。此外,29.54 GHz电磁波的波长大约是9.953 GHz电磁波波长的1/3,故29.54 GHz电磁波对外界环境更加敏感,由光学平台等金属物体的散射造成的气室位置处微波极化纯度进一步恶化,由文献[19]可知,当微波极化方向与激光偏振方向不一致时,三光子跃迁与双光子跃迁过程同时存在,会在谐振位置处出现另外一个探测光传输峰。图2(e)和图2(f)分别是处于 $|70S_{1/2}\rangle$ 态的铯原子在不同EIRP的2 GHz电磁波作用下产生的AC Stark频移光谱和频移量 ΔD_{Stark} 与 $\sqrt{M_{\text{EIRP}}}$ 的关系曲线。可以看出,与式(2)对应, ΔD_{Stark} 与 $\sqrt{M_{\text{EIRP}}}$ 存在明显的二次方对应关系。不同于谐振区,由于在远失谐区中Rydberg原子与外部电场的相互作用相对较弱,因此在远失谐区需要有场强更大的电磁波才能使EIT光谱发生明显偏移。

空间中的电场强度 $|E|$ ^[15]可以表示为

$$|E| = \Phi \frac{1}{\sqrt{2\pi c \epsilon_0}} \frac{\sqrt{M_{\text{EIRP}}}}{R}, \quad (3)$$

式中: c 是真空中的光速; ϵ_0 是自由空间介电常数; R 是天线口面到气室中激光光束的距离; Φ 是空间散射和原子气室内驻波扰动造成的衰减因子。

联立式(3)和式(1)或者式(2)可得

$$\begin{cases} \Delta D_{\text{AT}} = \Phi \frac{\mu}{2\pi\hbar \sqrt{2\pi c \epsilon_0} R} \sqrt{M_{\text{EIRP}}} \\ \Delta D_{\text{Stark}} = \Phi^2 \frac{\alpha_0 (2\pi \times f_{\text{MW}})}{8\pi c \epsilon_0 R^2} \left(\sqrt{M_{\text{EIRP}}} \right)^2. \end{cases} \quad (4)$$

将图2(b)、图2(d)和图2(f)中拟合曲线的系数与由Floquet理论^[2]计算得到的跃迁偶极矩或极化率进行对比,就可以得到谐振区或者远失谐区不同频率处的衰减因子。表1是不同微波频率对应的衰减因子对比。可以看出,衰减因子与电磁波频率成负相关性,这

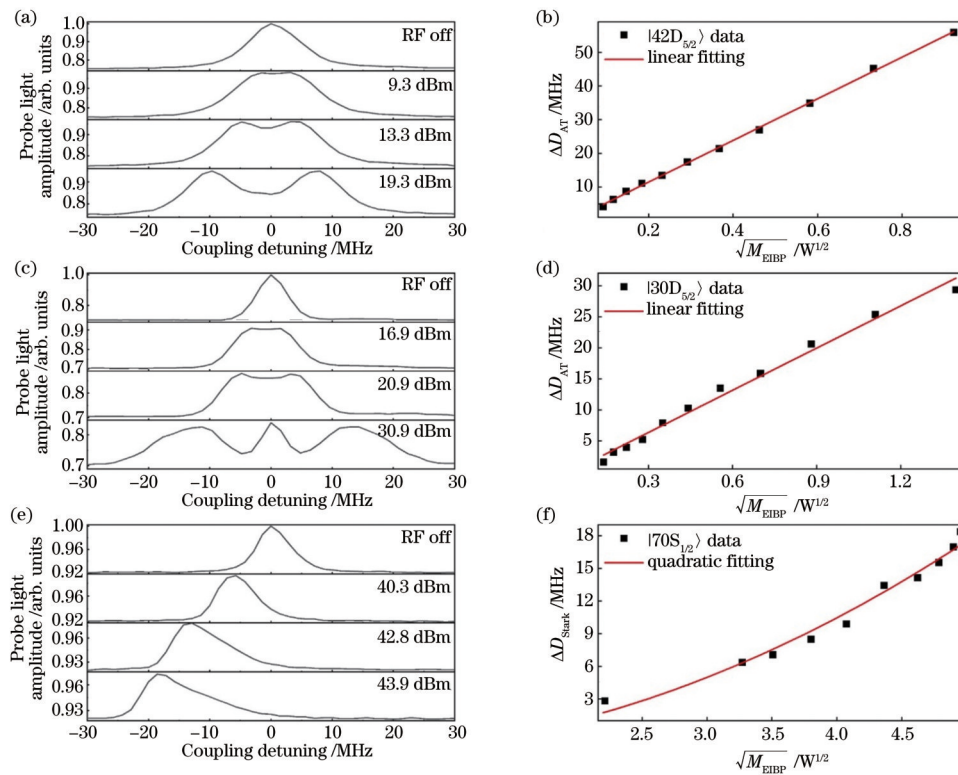


图2 不同Rydberg态铯原子在电磁波作用下的探测光传输光谱和偏移量与 $\sqrt{M_{EIRP}}$ 的关系。(a) $|42D_{5/2}\rangle$ Rydberg态铯原子在不同EIRP下9.953 GHz微波照射时的探测光传输光谱;(b) $|42D_{5/2}\rangle \rightarrow |43P_{3/2}\rangle$ 共振跃迁时 ΔD_{AT} 与 $\sqrt{M_{EIRP}}$ 的关系;(c) $|30D_{5/2}\rangle$ Rydberg态铯原子在不同EIRP下29.54 GHz微波照射时的探测光传输光谱;(d) $|30D_{5/2}\rangle \rightarrow |31P_{3/2}\rangle$ 共振跃迁时 ΔD_{AT} 与 $\sqrt{M_{EIRP}}$ 的关系;(e) $|70S_{1/2}\rangle$ Rydberg态铯原子在不同EIRP下2 GHz微波照射时的探测光传输光谱;(f) $|70S_{1/2}\rangle$ 态时 ΔD_{Stark} 与 $\sqrt{M_{EIRP}}$ 的关系

Fig. 2 Transmission spectra of probe light and relationship between offset and $\sqrt{M_{EIRP}}$ for cesium atom with different Rydberg states under electromagnetic wave irradiation. (a) Transmission spectra of probe light for cesium atom with $|42D_{5/2}\rangle$ Rydberg state under 9.953 GHz microwave illumination at different EIRPs; (b) relationship between ΔD_{AT} and $\sqrt{M_{EIRP}}$ for $|42D_{5/2}\rangle \rightarrow |43P_{3/2}\rangle$ resonance transition; (c) transmission spectra of probe light for cesium atom with $|30D_{5/2}\rangle$ Rydberg state under 29.54 GHz microwave illumination at different EIRPs; (d) relationship between ΔD_{AT} and $\sqrt{M_{EIRP}}$ for $|30D_{5/2}\rangle \rightarrow |31P_{3/2}\rangle$ resonance transition; (e) transmission spectra of probe light for cesium atom with $|70S_{1/2}\rangle$ Rydberg state under 2 GHz microwave illumination at different EIRPs; (f) relationship between ΔD_{Stark} and $\sqrt{M_{EIRP}}$ for $|70S_{1/2}\rangle$ state

表1 不同微波频率对应的衰减因子对比

Table 1 Comparison of attenuation factors corresponding to different microwave frequencies

RF frequency /GHz	$\alpha_0 / (\text{Hz} \cdot \text{V}^{-2} \cdot \text{m}^2)$	$\mu / (\text{C} \cdot \text{m})$	Fitting coefficient / $(\text{MHz} \cdot \text{W}^{-1/2})$	Φ
9.953	9.644×10^{-27}	61.711	0.339	
29.54	4.675×10^{-27}	22.677	0.125	
2	1.581×10^4	0.782	0.545	

是因为高频电磁波的波长与气室尺寸相当,高频电磁波容易在气室内部形成驻波,并且对空间环境更加

敏感。

3.2 调制射频场测量

Rydberg原子可以作为解调器自动地将调制电磁波中加载的基带信息解调出来^[30-35],具体地,当耦合光的频率锁定时,基带信号可以通过探测光幅度的变化进行提取。为验证Rydberg原子在宽带范围内对调制信号的感知能力,实验中将光电探测器的信号输出到分辨率带宽为1 Hz的频谱仪中,分别测量了远失谐区(2 GHz, $|70S_{1/2}\rangle$ 态, $M_{EIRP} = 36.9$ dBm)、近失谐区(9.5 GHz, $|42D_{5/2}\rangle$ 态, $M_{EIRP} = 30.2$ dBm)和谐振区(29.54 GHz, $|30D_{5/2}\rangle$ 态, $M_{EIRP} = 13.9$ dBm)中AM(调制深度为40%)和FM(调制带宽为-2.5~2.5 MHz)调制信号在不同调制频率下的解调信号SNR,结果如图3所示。光电探测器输出信号中有很

强的直流分量,实验中通过交流耦合来滤除直流分量,频谱仪的噪底受交流耦合的影响,呈现随频率由低到高逐渐减小的趋势。解调信号强度受Rydberg原子退相干时间的影响,随调制频率的升高逐渐降低。上述两种因素相互叠加,总体上来看,两种调制模式下的SNR随调制频率的升高呈现先增大后减小的趋势。受信号源最大调制频率的限制,载波频率为29.54 GHz的调制信号最高只测量到了1 MHz的调制频率,但通过SNR曲线的变化趋势可以看出,谐振区

信号所能达到的最大调制频率最高,近失谐区次之,远失谐区最低,这与三种情况下Rydberg原子对外部电场的敏感程度一致。最高调制频率受实验装置和参与作用原子数的影响,最终受限于Rydberg原子的退相干时间。本实验条件下的调制信号测量能力与相关文献的对比如表2所示。可以看出,在最大可探测调制频率相当的情况下,本文对Rydberg原子的响应区域和调制类型研究得更加全面。

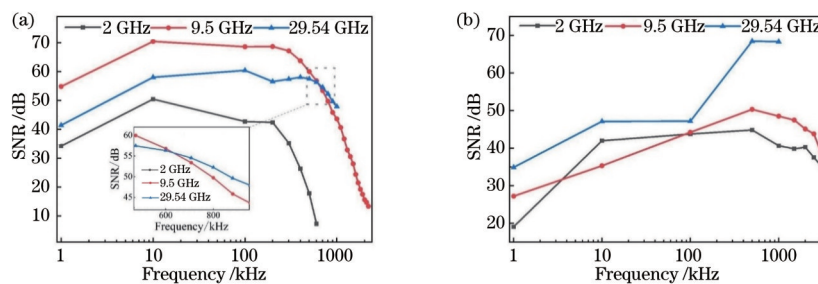


图3 不同载波频率的调制信号解调信号SNR与调制频率的关系。(a)调制深度为40%的AM测试结果;(b)调制带宽为-2.5~2.5 MHz的FM测试结果

Fig. 3 Demodulated signal SNR varying with modulation frequency under different carrier frequencies. (a) AM test results with 40% modulation depth; (b) FM test results with modulation bandwidth of -2.5~2.5 MHz

表2 相关文献调制信号测量能力对比

Table 2 Comparison of modulated signal measurement capabilities in related researches

Research	Response region	Modulation type	Maximum detected frequency /MHz
[30]	On-resonant	AM	4
[32]	On-resonant	AM	0.56
[34]	On-resonant	AM	2
This work	On/near/off-resonant	AM/FM	2.5/3.0

为进一步验证Rydberg原子在超宽带范围内对调制射频信号的连续测量能力,用调制深度为40%,调制频率为10 kHz的AM调制信号照射处于不同Rydberg态的铯原子,得到100 kHz~40 GHz的超宽带范围内不同载波频率下的解调信号SNR变化曲线,如图4所示。对于2 GHz以下的载波,选用 $|70S_{1/2}\rangle$ 态。对于2~20 GHz的载波,选用 $|42D_{5/2}\rangle$ 态。对于20~40 GHz的载波,选用 $|30D_{5/2}\rangle$ 态。同时,在每个频点处通过调节载波信号的EIRP来获取最优SNR。可以看

出,在100 kHz~40 GHz的超宽带范围内,解调信号SNR都保持在10 dB以上,并且在10 GHz和30 GHz附近 $|42D_{5/2}\rangle \rightarrow |43P_{3/2}\rangle$ 和 $|30D_{5/2}\rangle \rightarrow |31P_{3/2}\rangle$ 谐振跃迁的存在会造成两个极大值区域。在非谐振区中,由于EIT谱的变化不再与电场强度呈线性关系,且受限于信号源最大输出功率,故非谐振区的SNR要比谐振区低。此外,在非谐振区某些频点处,光学平台等金属物体的散射和气室内驻波的影响会造成SNR的抬高或降低。

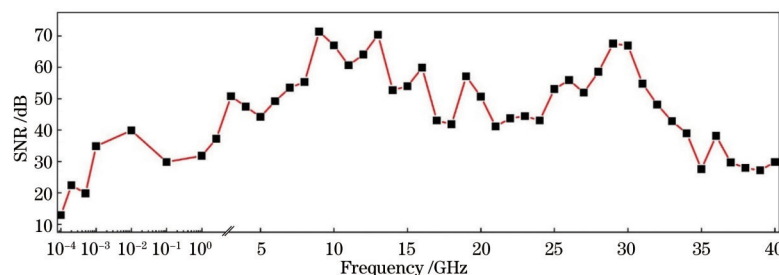


图4 调制深度为40%,调制频率为10 kHz的AM调制信号在不同载波频率下的解调信号SNR

Fig. 4 Demodulated signal SNRs of AM modulation signal with modulation depth of 40% and modulation frequency of 10 kHz under different carrier frequencies

4 结 论

通过调节耦合光波长使室温铯原子处于 $|70S_{1/2}\rangle$ 、 $|42D_{5/2}\rangle$ 和 $|30D_{5/2}\rangle$ 三个不同的Rydberg能级。利用谐振区的EIT-AT效应和非谐振区的AC Stark效应，分别测量了谐振区(9.953 GHz/29.54 GHz)和远失谐区(2 GHz)电磁波的电场强度，并与信号等效全向辐射功率对比，得到了不同频率处空间散射和气室内驻波扰动引起的衰减因子。为验证Rydberg原子在宽带范围内的通信能力，分别测量了谐振区、近失谐区和远失谐区AM/FM调制的射频信号在不同调制频率下的解调信号SNR。在此基础上，进一步用调制深度为40%，调制频率为10 kHz的AM调制信号在100 kHz~40 GHz的超宽带载波范围内实现调制信号的连续探测。实验结果表明，Rydberg原子具有超宽带范围内的电场感知和通信应用能力，是实现新一代射频信号量子感知的重要手段。

参 考 文 献

- [1] Chu L J. Physical limitations of omni-directional antennas [J]. Journal of Applied Physics, 1948, 19(12): 1163-1175.
- [2] Yoshida S, Reinhold C O, Burgdörfer J, et al. Photoexcitation of $n \approx 305$ Rydberg states in the presence of an rf drive field[J]. Physical Review A, 2012, 86(4): 043415.
- [3] Sedlacek J A, Schwettmann A, Kübler H, et al. Microwave electrometry with Rydberg atoms in a vapour cell using bright atomic resonances[J]. Nature Physics, 2012, 8(11): 819-824.
- [4] Kumar S, Fan H, Kübler H, et al. Atom-based sensing of weak radio frequency electric fields using homodyne readout[J]. Scientific Reports, 2017, 7: 42981.
- [5] Liao K Y, Tu H T, Yang S Z, et al. Microwave electrometry via electromagnetically induced absorption in cold Rydberg atoms[J]. Physical Review A, 2020, 101(5): 053432.
- [6] Ripka F, Amarloo H, Erskine J, et al. Application-driven problems in Rydberg atom electrometry[J]. Proceedings of SPIE, 2021, 11700: 117002Y.
- [7] Thaicharoen N, Moore K R, Anderson D A, et al. Electromagnetically-induced transparency, absorption, and microwave field sensing in a Rb vapor cell with a three-color all-infrared laser system[J]. Physical Review A, 2019, 100(6): 063427.
- [8] 廖开宇, 涂海涛, 张新定, 等. 基于里德堡原子的微波传感与通信[J]. 中国科学: 物理学 力学 天文学, 2021, 51(7): 074202.
- Liao K Y, Tu H T, Zhang X D, et al. Rydberg atom based microwave sensing and communication[J]. Scientia Sinica (Physica, Mechanica & Astronomica), 2021, 51(7): 074202.
- [9] Jing M Y, Hu Y, Ma J, et al. Atomic superheterodyne receiver based on microwave-dressed Rydberg spectroscopy[J]. Nature Physics, 2020, 16(9): 911-915.
- [10] Gordon J A, Simons M T, Haddab A H, et al. Weak electric-field detection with sub-1 Hz resolution at radio frequencies using a Rydberg atom-based mixer[J]. AIP Advances, 2019, 9(4): 045030.
- [11] Hao L P, Xue Y M, Fan J B, et al. Precise measurement of a weak radio frequency electric field using a resonant atomic probe[J]. Chinese Physics B, 2020, 29(3): 033201.
- [12] 樊佳蓓, 郝丽萍, 白景旭, 等. 基于Rydberg原子的高灵敏微波探测与通信[J]. 物理学报, 2021, 70(6): 063201.
- Fan J B, Hao L P, Bai J X, et al. High-sensitive microwave sensor and communication based on Rydberg atoms[J]. Acta Physica Sinica, 2021, 70(6): 063201.
- [13] Liu X B, Jia F D, Zhang H Y, et al. Using amplitude modulation of the microwave field to improve the sensitivity of Rydberg-atom based microwave electrometry[J]. AIP Advances, 2021, 11(8): 085127.
- [14] Jia F D, Liu X B, Mei J, et al. Span shift and extension of quantum microwave electrometry with Rydberg atoms dressed by an auxiliary microwave field[J]. Physical Review A, 2021, 103(6): 063113.
- [15] Robinson A K, Artusio-Glimpse A B, Simons M T, et al. Atomic spectra in a six-level scheme for electromagnetically induced transparency and Autler-Townes splitting in Rydberg atoms[J]. Physical Review A, 2021, 103(2): 023704.
- [16] Simons M T, Artusio-Glimpse A B, Holloway C L, et al. Continuous radio-frequency electric-field detection through adjacent Rydberg resonance tuning[J]. Physical Review A, 2021, 104(3): 032824.
- [17] Prajapati N, Robinson A K, Berweger S, et al. Enhancement of electromagnetically induced transparency based Rydberg-atom electrometry through population repumping[J]. Applied Physics Letters, 2021, 119(21): 214001.
- [18] Anderson D A, Paradis E G, Raithel G. A vapor-cell atomic sensor for radio-frequency field detection using a polarization-selective field enhancement resonator[J]. Applied Physics Letters, 2018, 113(7): 073501.
- [19] Sedlacek J A, Schwettmann A, Kübler H, et al. Atom-based vector microwave electrometry using rubidium Rydberg atoms in a vapor cell[J]. Physical Review Letters, 2013, 111(6): 063001.
- [20] Bussey L W, Winterburn A, Menchetti M, et al. Rydberg RF receiver operation to track RF signal fading and frequency drift[J]. Journal of Lightwave Technology, 2021, 39(24): 7813-7820.
- [21] Simons M T, Haddab A H, Gordon J A, et al. A Rydberg atom-based mixer: measuring the phase of a radio frequency wave[J]. Applied Physics Letters, 2019, 114(11): 114101.
- [22] Anderson D A, Sapiro R E, Gonçalves L F, et al. Atom radio-frequency interferometry[EB/OL]. (2020-10-26) [2022-01-06]. <https://arxiv.org/abs/2010.13657>.
- [23] Robinson A K, Prajapati N, Senic D, et al. Determining the angle-of-arrival of a radio-frequency source with a Rydberg atom-based sensor[J]. Applied Physics Letters,

- 2021, 118(11): 114001.
- [24] Simons M T, Gordon J A, Holloway C L. Fiber-coupled vapor cell for a portable Rydberg atom-based radio frequency electric field sensor[J]. *Applied Optics*, 2018, 57(22): 6456-6460.
- [25] Holloway C L, Gordon J A, Jefferts S, et al. Broadband Rydberg atom-based electric-field probe for SI-traceable, self-calibrated measurements[J]. *IEEE Transactions on Antennas and Propagation*, 2014, 62(12): 6169-6182.
- [26] Cardman R, Gonçalves L F, Sapiro R E, et al. Atomic 2D electric field imaging of a Yagi-Uda antenna near-field using a portable Rydberg-atom probe and measurement instrument[J]. *Advanced Optical Technologies*, 2020, 9(5): 305-312.
- [27] Holloway C L, Simons M T, Haddab A H, et al. A multiple-band Rydberg atom-based receiver: AM/FM stereo reception[J]. *IEEE Antennas and Propagation Magazine*, 2021, 63(3): 63-76.
- [28] Meyer D H, Castillo Z A, Cox K C, et al. Assessment of Rydberg atoms for wideband electric field sensing[J]. *Journal of Physics B*, 2020, 53(3): 034001.
- [29] Meyer D H, Kunz P D, Cox K C. Waveguide-coupled Rydberg spectrum analyzer from 0 to 20 GHz[J]. *Physical Review Applied*, 2021, 15(1): 014053.
- [30] Meyer D H, Cox K C, Fatemi F K, et al. Digital communication with Rydberg atoms and amplitude-modulated microwave fields[J]. *Applied Physics Letters*, 2018, 112(21): 211108.
- [31] Cox K C, Meyer D H, Fatemi F K, et al. Quantum-limited atomic receiver in the electrically small regime[J]. *Physical Review Letters*, 2018, 121(11): 110502.
- [32] Otto J S, Hunter M K, Kjærgaard N, et al. Data capacity scaling of a distributed Rydberg atomic receiver array[J]. *Journal of Applied Physics*, 2021, 129(15): 154503.
- [33] Anderson D A, Sapiro R E, Raithel G. An atomic receiver for AM and FM radio communication[J]. *IEEE Transactions on Antennas and Propagation*, 2021, 69(5): 2455-2462.
- [34] Song Z F, Liu H P, Liu X C, et al. Rydberg-atom-based digital communication using a continuously tunable radio-frequency carrier[J]. *Optics Express*, 2019, 27(6): 8848-8857.
- [35] Holloway C L, Simons M T, Gordon J A, et al. Detecting and receiving phase-modulated signals with a Rydberg atom-based receiver[J]. *IEEE Antennas and Wireless Propagation Letters*, 2019, 18(9): 1853-1857.
- [36] Jau Y Y, Carter T. Vapor-cell-based atomic electrometry for detection frequencies below 1 kHz[J]. *Physical Review Applied*, 2020, 13(5): 054034.
- [37] Anderson D A, Paradis E, Raithel G, et al. High-resolution antenna near-field imaging and sub-THz measurements with a small atomic vapor-cell sensing element[C]//11th Global Symposium on Millimeter Waves (GSMM), May 22-24, 2018, Boulder, CO, USA. New York: IEEE Press, 2018: 18042205.
- [38] 李伟, 张淳刚, 张好, 等. 基于里德伯原子AC-Stark效应的工频电场测量[J]. 激光与光电子学进展, 2021, 58(17): 1702002.
- Li W, Zhang C G, Zhang H, et al. Power-frequency electric field measurement based on AC-Stark effect of Rydberg atoms[J]. *Laser & Optoelectronics Progress*, 2021, 58(17): 1702002.
- [39] 吉经纬, 程鹤楠, 张镇, 等. 可搬运铷喷泉原子钟全自动激光稳频系统[J]. 光学学报, 2020, 40(22): 2214002.
- Ji J W, Cheng H N, Zhang Z, et al. Automatic laser frequency stabilization system for transportable ⁸⁷Rb fountain clock[J]. *Acta Optica Sinica*, 2020, 40(22): 2214002.
- [40] 洪毅, 侯霞, 陈迪俊, 等. 基于Rb⁸⁷调制转移光谱稳频技术研究[J]. 中国激光, 2021, 48(21): 2101003.
- Hong Y, Hou X, Chen D J, et al. Research on frequency stabilization technology of modulation transfer spectroscopy based on Rb⁸⁷[J]. *Chinese Journal of Lasers*, 2021, 48(21): 2101003.